Nondipole effects in photon emission by laser-driven ions

C. C. Chirilă, N. J. Kylstra, and R. M. Potvliege
Department of Physics, University of Durham, Durham DH1 3LE, United Kingdom

C. J. Joachain
Physique Théorique CP 227, Université Libre de Bruxelles, B–1050 Brussels, Belgium
and Max-Planck-Institute für Quantenoptik, D-85748 Garching, Germany
(Received 19 September 2002; published 20 December 2002)

The influence of the magnetic-field component of the incident pulse on the emission of photons by multiply charged ions interacting with intense, near-infrared laser pulses is investigated theoretically using a strong-field approximation that treats the coupling of the atom with the incident field beyond the dipole approximation. For peak pulse intensities approaching 10^{17} W cm^{-2}, the electron drift in the laser propagation direction due to the magnetic-field component of the incident pulse strongly influences the photon emission spectra. In particular, emission is reduced and the plateau structure of the spectra modified, as compared to the predictions in the dipole approximation. Nondipole effects become more pronounced as the ionization potential of the ion increases. Photon emission spectra are interpreted by analysing classical electron trajectories within the semiclassical recollision model. It is shown that a second pulse can be used to compensate the magnetic-field induced drift for selected trajectories so that, in a well-defined spectral region, a single attosecond pulse is emitted by the ion.

DOI: 10.1103/PhysRevA.66.063411 PACS number(s): 42.50.Hz, 32.80.Rm, 42.65.Ky

I. INTRODUCTION

Atoms and ions interacting with intense infrared laser pulses emit high-order harmonics of the driving field in the form of coherent attosecond pulses [1–6]. This process is readily understood in terms of the semiclassical recollision, or ''Simpleman's model,'' whereby electrons are detached from their parent atom or ion by quasistatic tunneling ionization, oscillate in the field, and return to the core where they radiatively recombine [7–11]. A fully quantum version of this model has formed the basis of a vast number of theoretical investigations of high-order-harmonic generation [10–12], and has been used successfully to analyze experiment (see, e.g., Ref. [13]). This theory relies on the strong-field approximation (SFA), which assumes that the interaction of the detached electron with the field is much stronger than its interaction with the core so that the latter can be neglected. In addition to explaining high-order-harmonic generation, the model also forms the basis of our present understanding of other processes occurring in low-frequency laser fields, such as high-order above threshold ionization (ATI) and recollision-induced multiple ionization.

Once detached, the electron is accelerated by both the electric-field and magnetic-field components of the incident beam. The magnetic-field component tends to deflect the trajectory towards the direction of propagation of the beam, with the result that the electron never returns to the nucleus if detached with zero velocity. The drift in the propagation direction imparted by the Lorentz force is largely offset by the width of the returning wave packet, and is therefore negligible at the intensities and wavelengths normally used in experiments on high-order-harmonic generation (typically 10^{14}–10^{15} W cm^{-2} in the visible or near infrared). In these conditions, the Lorentz force does not need to be taken into account and the coupling of the electron with the incident field is accurately described within the dipole approximation. However, at much higher intensities the drift is no longer negligible and the dipole approximation ceases to be valid. Moreover, the electron's dynamics becomes relativistic at very high intensities. (At the Ti:sapphire wavelength, 800 nm, the ratio of the nonrelativistic ponderomotive energy of the electron to its rest energy exceeds unity for an intensity of 8.5×10^{18} W cm^{-2}.)

Recent theoretical investigations of atomic stabilization in the high-frequency stabilization regime [14–18] and of photon emission by ions interacting with intense near-infrared laser pulses [19–24] have established the existence of a ''nondipole nonrelativistic'' dynamical regime, in which the effect of the magnetic-field component of the laser is too large for the dipole approximation to be appropriate but not so large that a relativistic description is necessary. At the Ti:sapphire wavelength, the dipole approximation is expected to remain valid up to intensities of about 5×10^{16}–1×10^{17} W cm^{-2} (depending on the system, as will be seen below). Due to the magnetic drift, the probability that the electron recombines with the core is non-negligible only if the electron is initially detached with a nonzero velocity in the direction opposite to the propagation direction of the incident beam. However, the detachment probability falls off rapidly if this initial velocity departs from zero [25,26]. The consequence is that the harmonic generation is weaker and varies differently as a function of the frequency of the emitted photon than would be the case in the absence of the Lorentz force.

The dipole approximation has been assumed in nearly all the theoretical work to date on high-order-harmonic generation in low-frequency fields. Only a few fully quantum calculations, all based on the strong-field approximation, have addressed the role of the magnetic drift in this context. Expressions for the dipole moment of an atom or ion in the

nondipole nonrelativistic regime have been developed by Walser *et al*. [21] and, in another form, by us [22,27], and applied to emission driven by ultrashort pulses. A relativistic formulation of harmonic generation in stationary fields, based on the Klein-Gordon equation, has also been given by Milošević, Hu, and Becker [20,24].

In the present paper, we give a detailed account of the nondipole SFA sketched in Ref. [22] and relate it to the theory of Walser *et al*. [21]. We also assess the importance of the relativistic effects neglected in our approach by comparing with results obtained by Milošević, Hu, and Becker [20]. We consider, in particular, the emission of photons by isolated Li^{2+}, Be^{3+}, and Ne^{6+} ions exposed to strong near-infrared pulses. We do not study emission from neutrals, as only multicharged ions can withstand the intensities at which the magnetic drift becomes significant without ionizing immediately. The importance of the nondipole effects is investigated by comparing the nondipole nonrelativistic photon emission spectra with dipole spectra for long pulses (represented by stationary fields) as well as for few-cycle pulses. The numerical results are interpreted with the help of the recollision model, generalized to the nondipole case. The trajectories we consider are real and obey the classical equations of motion. This approach complements the description of the electron's dynamics in terms of complex trajectories discussed in Ref. [20]; the two approaches lead to essentially the same physical picture. Finally, we illustrate how a second, weak laser pulse can be used to compensate for the magnetic drift of the electron. In particular, we show that the recombination probability of selected electron trajectories can be enhanced by several orders of magnitude in this way, thereby leading to photon emission in the form of a single attosecond x-ray pulse. Unless otherwise indicated, atomic units are used throughout the paper.

II. THEORETICAL APPROACH

A. Nondipole nonrelativistic approximation

We assume that the vector potential describing the laser field can be written as

$$\mathbf{A}(\eta)=\hat{\boldsymbol{\epsilon}}(\mathcal{E}/\omega)f(\eta)\sin(\eta), \tag{1}$$

with $\eta=\omega(t-\hat{\mathbf{k}}\cdot\mathbf{r}/c)$. The field has a carrier wavelength $\lambda=2\pi c/\omega$, field strength $\mathcal{E}$, is linearly polarized with polarization vector $\hat{\boldsymbol{\epsilon}}$, and propagates in the direction $\hat{\mathbf{k}}$. The function $f(\eta)$ describes the temporal profile of the pulse; $f(\eta)\equiv 1$ for a stationary field.

The influence of the magnetic-field component of the laser on the electron dynamics can be accounted for in the long-wavelength and nonrelativistic regime considered here by expanding the vector potential to first order in $1/c$. Assuming the atom to be initially located at the origin leads to

$$\mathbf{A}(\eta)\simeq\mathbf{A}(\omega t)+\frac{1}{c}(\hat{\mathbf{k}}\cdot\mathbf{r})\mathbf{E}(\omega t), \tag{2}$$

where $\mathbf{E}(\omega t)=-(d/dt)\mathbf{A}(\omega t)=-\hat{\boldsymbol{\epsilon}}(d/dt)A(\omega t)=\hat{\boldsymbol{\epsilon}}E(\omega t)$. Our work is based on the time-dependent Schrödinger equation

$$i\frac{\partial}{\partial t}\Psi(\mathbf{r},t)=\left(\frac{1}{2}[-i\boldsymbol{\nabla}+\mathbf{A}(\omega t)]^2+\frac{1}{c}(\hat{\mathbf{k}}\cdot\mathbf{r})[-i\boldsymbol{\nabla}+\mathbf{A}(\omega t)]\cdot\mathbf{E}(\omega t)+V(r)\right)\Psi(\mathbf{r},t), \tag{3}$$

which is exact up to order $1/c$ in the atom-field interaction. We neglect the spin of the electron. The potential $V(r)$ describes the interaction of the electron with the ionic core. There are two nondipole terms in the Hamiltonian: the first one, in $\boldsymbol{\nabla}\cdot\mathbf{E}(\omega t)$, gives rise to electric quadrupole and magnetic dipole transitions. The second one, in $\mathbf{A}(\omega t)\cdot\mathbf{E}(\omega t)$, contributes to the drift in the propagation direction induced by the magnetic-field component of the incident beam and has a large influence on the emission of photons by ions at high laser intensities.

At low frequencies, it is appropriate to transform the time-dependent Schrödinger equation to the length gauge, with the result

$$i\frac{\partial}{\partial t}\Psi_{\mathrm{L}}(\mathbf{r},t)=\left(-\frac{1}{2}\nabla^2+\left[\mathbf{r}-\frac{i}{c}(\hat{\mathbf{k}}\cdot\mathbf{r})\boldsymbol{\nabla}\right]\cdot\mathbf{E}(\omega t)+V(r)\right)\Psi_{\mathrm{L}}(\mathbf{r},t), \tag{4}$$

where $\Psi_{\mathrm{L}}(\mathbf{r},t)=\exp[i\mathbf{A}(\omega t)\cdot\mathbf{r}]\Psi(\mathbf{r},t)$. By introducing the retarded Green's function associated with the Hamiltonian of Eq. (4), the wave function $\Psi_{\mathrm{L}}(\mathbf{r},t)$ can be obtained as the solution of a time-dependent Lippmann-Schwinger equation. In the SFA approach of Lewenstein and co-workers [1,10], this Green's function is replaced by the Volkov Green's function associated with the Hamiltonian that describes a free electron in the laser field, $G_{\mathrm{V}}^{(+)}(\mathbf{r},t;\mathbf{r}',t')$. To account for the magnetic-field component of the laser pulse at high intensities, we employ the nondipole Volkov Green's function discussed in the Appendix. Neglecting continuum-continuum transitions [28], the dipole moment of the atom then reduces to

$$\mathbf{d}(t)\simeq\int_{-\infty}^{t}dt'\int d\mathbf{r}d\mathbf{r}'\,\phi_0^*(\mathbf{r},t)\times(-\mathbf{r})G_{\mathrm{V}}^{(+)}(\mathbf{r},t;\mathbf{r}',t')H_{\mathrm{int}}(t')\phi_0(\mathbf{r}',t')+\mathrm{c.c.} \tag{5}$$

The atom or ion is initially in its ground state and is described by the wave function $\phi_0(\mathbf{r},t)=\phi_0(\mathbf{r})\exp(iI_pt)$, I_p being the ionization potential of the state. $H_{\mathrm{int}}(t')$ is the atom-field interaction Hamiltonian

$$H_{\mathrm{int}}(t')=\left[\mathbf{r}-\frac{i}{c}(\hat{\mathbf{k}}\cdot\mathbf{r})\boldsymbol{\nabla}\right]\cdot\mathbf{E}(\omega t'). \tag{6}$$

Equation (5) can also be written in the form

$$\mathbf{d}(t) \simeq 2\,\mathrm{Im}\int_0^t dt' \int d\mathbf{p}\,\mathbf{d}_{\mathrm{rec}}^*[\boldsymbol{\pi}(\mathbf{p},t)] \times \exp[-iS(\mathbf{p},t,t')]\,d_{\mathrm{ion}}[\boldsymbol{\pi}(\mathbf{p},t'),t'], \tag{7}$$

where

$$\boldsymbol{\pi}(\mathbf{p},t) = \mathbf{p} + \mathbf{A}(\omega t) + \frac{1}{c}\left[\mathbf{p}\cdot\mathbf{A}(\omega t) + \frac{1}{2}A^2(\omega t)\right]\hat{\mathbf{k}}, \tag{8}$$

$$S(\mathbf{p},t,t') = \frac{1}{2}\int_{t'}^{t} dt''[\boldsymbol{\pi}(\mathbf{p},t'')]^2 + I_p(t-t'), \tag{9}$$

$$\mathbf{d}_{\mathrm{rec}}(\mathbf{q}) = (2\pi)^{-3/2}\int d\mathbf{r} e^{-i\mathbf{q}\cdot\mathbf{r}}(-\mathbf{r})\,\phi_0(\mathbf{r}), \tag{10}$$

and

$$d_{\mathrm{ion}}(\mathbf{q},t) = (2\pi)^{-3/2}\int d\mathbf{r} e^{-i\mathbf{q}\cdot\mathbf{r}} H_{\mathrm{int}}(t)\,\phi_0(\mathbf{r}). \tag{11}$$

The spectrum of the emitted photons is then obtained by calculating $|\hat{\boldsymbol{\epsilon}}\cdot\mathbf{a}(\Omega)|^2$, for emission polarized parallel to the polarization direction of the incident pulse, and $|\hat{\mathbf{k}}\cdot\mathbf{a}(\Omega)|^2$, for emission polarized along the direction of propagation of the incident pulse. In these expressions, Ω denotes the angular frequency of the emitted photon and $\mathbf{a}(\Omega)$ the Fourier transform of $\ddot{\mathbf{d}}(t)$. The ratio Ω/ω is an effective ''harmonic order.'' Results in the dipole approximation are obtained by setting $1/c=0$. The SFA is readily modified to include the depletion of the ground state [1,10]; however we can neglect depletion for the laser parameters and atomic systems considered here.

B. Saddle-point integration

The quasiclassical action $S(\mathbf{p},t,t')$ is a rapidly varying function of $\mathbf{p}$, t, and t', and therefore the required integrations in Eq. (7) can be carried out using the saddle-point method. We proceed by first using the relation

$$d_{\mathrm{ion}}[\boldsymbol{\pi}(\mathbf{p},t'),t'] = -i\frac{d}{dt'}\int \frac{d\mathbf{r}}{(2\pi)^{3/2}} e^{-i\boldsymbol{\pi}(\mathbf{p},t')\cdot\mathbf{r}}\phi_0(\mathbf{r}) = -i\frac{d}{dt'}\tilde{\phi}[\boldsymbol{\pi}(\mathbf{p},t')], \tag{12}$$

where

$$\tilde{\phi}[\boldsymbol{\pi}(\mathbf{p},t')] = \frac{(8I_{\mathrm{p}})^{5/4}}{8\pi}\frac{1}{[\boldsymbol{\pi}^2(\mathbf{p},t')/2 + I_{\mathrm{p}}]^2} = \frac{(8I_{\mathrm{p}})^{5/4}}{8\pi}\left[-\frac{\partial}{\partial t'}S(\mathbf{p},t,t')\right]^{-2} \tag{13}$$

is the Fourier transform of the ground-state wave function of the ion. We have assumed that $V(r)$ is a Coulomb potential with effective nuclear charge $(2I_{\mathrm{p}})^{1/2}$. Equation (7) is then integrated by parts. Since $H_{\mathrm{int}}(t'=0)=0$, the boundary term at $t'=0$ is zero while the boundary term at $t'=t$ can be ignored; it corresponds to the process whereby the electron both ionizes and recombines at time t. Next, the integral over $\mathbf{p}$ is approximated using the saddle-point method, with the result

$$\mathbf{d}(t) \simeq 2\,\mathrm{Im}\frac{(8I_{\mathrm{p}})^{5/4}}{8\pi}\int_0^t dt' C(\tau)\,\mathbf{d}_{\mathrm{rec}}^*[\boldsymbol{\pi}(\mathbf{p}_{\mathrm{s}},t)] \times \exp[-iS(\mathbf{p}_{\mathrm{s}},t,t')]\left[\frac{\partial}{\partial t'}S(\mathbf{p}_{\mathrm{s}},t,t')\right]^{-1}. \tag{14}$$

The saddle momentum $\mathbf{p}_{\mathrm{s}}$ depends on t and t' and is obtained by solving

$$\boldsymbol{\nabla}_{\mathbf{p}} S(\mathbf{p},t,t')\big|_{\mathbf{p}=\mathbf{p}_{\mathrm{s}}} = 0. \tag{15}$$

The factor

$$C(\tau) = (2\pi)^{3/2}\left((\varepsilon + i\tau)^3\left[1 - \frac{1}{c^2}(\hat{\boldsymbol{\epsilon}}\cdot\mathbf{p}_{\mathrm{s}})^2\right]\right)^{-1/2}, \tag{16}$$

with $\tau = t - t'$ and ε a small positive parameter, can be understood physically as arising from wave-packet spreading.

The integral over t' in Eq. (14) is straightforward to evaluate numerically. However, the integration must be repeated for each value of t, due to the dependence of the integrand on t. The total computational effort required for calculating the temporal variation of the dipole moment thus increases as the square of the laser-pulse duration. For this reason, and because of the rapid oscillations of the exponential term, it is advantageous to calculate the integral using the saddle-point method. The saddle times t_{s} are complex and are determined by the equation

$$-\frac{\partial}{\partial t'}S(\mathbf{p}_{\mathrm{s}},t,t')\big|_{t'=t_{\mathrm{s}}} = [\pi^2(\mathbf{p}_{\mathrm{s}},t')/2 + I_{\mathrm{p}}]\big|_{t'=t_{\mathrm{s}}} = 0. \tag{17}$$

Expanding the denominator in Eq. (14) in a Taylor series, retaining only the linear term, and noting that the integrand has a first-order pole at the saddle times [29], the dipole moment is found to be

$$\mathbf{d}(t) \simeq -2\,\mathrm{Re}\frac{(8I_{\mathrm{p}})^{5/4}}{8}\sum_{t_{\mathrm{s}}} C(t-t_{\mathrm{s}})\,\mathbf{d}_{\mathrm{rec}}^*[\boldsymbol{\pi}(\mathbf{p}_{\mathrm{s}},t)] \times \exp[-iS(\mathbf{p}_{\mathrm{s}},t,t_{\mathrm{s}})]\left[\boldsymbol{\pi}(\mathbf{p}_{\mathrm{s}},t')\cdot\frac{\partial}{\partial t'}\boldsymbol{\pi}(\mathbf{p}_{\mathrm{s}},t')\right]^{-1}_{t'=t_{\mathrm{s}}}. \tag{18}$$

In all the cases considered, we have found that the spectra calculated using Eq. (18) are in very good agreement with those obtained by carrying out the integration over t' in Eq.

(14) numerically. Typically, they differ by less than a factor of 2, and the agreement improves as the laser intensity increases.

The saddle time can also be obtained using a semianalytical approach, similar to that described by Ivanov, Brabec, and Burnett [30] for calculations in the dipole approximation. In this approach, the saddle time is expressed as $t_s = t_d + \Delta$, with t_d determined by solving

$$\pi_\epsilon(\mathbf{p}_s, t_d) = \hat{\boldsymbol{\epsilon}} \cdot \boldsymbol{\pi}(\mathbf{p}_s, t_d) = 0. \tag{19}$$

Equation (17) is then expanded in powers of Δ,

$$-\frac{\partial}{\partial t'} S(\mathbf{p}_s, t, t')|_{t'=t_s} = s_0 + s_1\Delta + \tfrac{1}{2}s_2\Delta^2 + O(\Delta^3). \tag{20}$$

In terms of the component of $\boldsymbol{\pi}(\mathbf{p}_s, t_d)$ in the propagation direction,

$$\pi_k(\mathbf{p}_s, t_d) = \hat{\mathbf{k}} \cdot \boldsymbol{\pi}(\mathbf{p}_s, t_d) = -\frac{1}{2c(t-t_d)} \int_{t_d}^{t} dt'' |\mathbf{A}(\omega t'') - \mathbf{A}(\omega t_d)|^2, \tag{21}$$

the first coefficient is

$$s_0 = I_p + \tfrac{1}{2}\pi_k^2(\mathbf{p}_s, t_d). \tag{22}$$

Analytical expressions for s_1 and s_2 are lengthy, and in practice can be obtained numerically. Setting Eq. (20) equal to zero and solving for Δ, the dipole moment (18) is evaluated using

$$S(\mathbf{p}_s, t, t_s) \simeq S(\mathbf{p}_s, t, t_d) - s_0\Delta - \tfrac{1}{2}s_1\Delta^2 - \tfrac{1}{6}s_2\Delta^3 \tag{23}$$

and

$$\left[\boldsymbol{\pi}(\mathbf{p}_s, t') \cdot \frac{\partial}{\partial t'} \boldsymbol{\pi}(\mathbf{p}_s, t') \right]_{t'=t_s} \simeq s_1 + \Delta s_2. \tag{24}$$

We have verified that this approach yields results that are for all practical purposes identical to those derived using Eqs. (17) and (18).

The calculations can be simplified even further by neglecting terms of order $1/c^2$ and higher in the saddle momentum. In this approximation

$$\mathbf{p}_s = -\frac{\alpha_1(t,t')}{t-t'}\hat{\boldsymbol{\epsilon}} + \frac{1}{c}\left[\frac{\alpha_1^2(t,t')}{(t-t')^2} - \frac{\alpha_2(t,t')}{2(t-t')} \right] \hat{\mathbf{k}}, \tag{25}$$

where

$$\alpha_n(t,t') = \int_{t'}^{t} dt'' A^n(t''). \tag{26}$$

This means that $\boldsymbol{\pi}(\mathbf{p}_s, t_d)$ and $S(\mathbf{p}_s, t, t_d)$, respectively, will be correct to order $1/c$ and $1/c^2$. Using Eq. (25), Eq. (19) reduces to

$$\int_{t_d}^{t} dt'' [\mathbf{A}(\omega t'') - \mathbf{A}(\omega t_d)] = 0, \tag{27}$$

thereby giving t_d in the dipole approximation. The coefficients s_1 and s_2, to order $1/c^2$, are then found to be

$$s_1 = \frac{\pi_k^2(\mathbf{p}_s, t_d)}{t - t_d}, \tag{28}$$

$$s_2 = E^2(\omega t_d)\left[1 + \frac{1}{c}\pi_k(\mathbf{p}_s, t_d) \right] + \frac{3s_1}{t - t_d}. \tag{29}$$

Note that all of the nondipole corrections to the expansion coefficients s_i are of order $1/c^2$. Hence, consistent with the action being correct to order $1/c^2$, we set

$$s_1 = 0, \quad s_2 = E^2(\omega t_d). \tag{30}$$

The resulting dipole moment can be expressed as [21,30]

$$\mathbf{d}(t) \simeq -2\,\mathrm{Im} \sum_{t_d} \mathbf{a}_{\mathrm{rec}}^*(t, t_d) a_{\mathrm{pr}}(t, t_d) a_{\mathrm{ion}}(t, t_d), \tag{31}$$

with the ionization, propagation, and recombination amplitudes, respectively, given by

$$a_{\mathrm{ion}}(t, t_d) = \frac{(8I_p)^{5/4}}{8(2s_0 s_2)^{1/2}} \exp\left[-\frac{1}{3}\left(\frac{8s_0^3}{s_2} \right)^{1/2} \right], \tag{32}$$

$$a_{\mathrm{pr}}(t, t_d) = C(t - t_s) \exp[-iS(\mathbf{p}_s, t, t_d)], \tag{33}$$

$$\mathbf{a}_{\mathrm{rec}}^*(t, t_d) = \mathbf{d}_{\mathrm{rec}}^*[\boldsymbol{\pi}(\mathbf{p}_s, t)]. \tag{34}$$

We have evaluated the accuracy of the formula (31) by calculating $|\hat{\boldsymbol{\epsilon}} \cdot \mathbf{a}(\Omega)|^2$ and comparing with the results obtained using exact numerical complex saddle times t_s in Eq. (18), for the laser parameters and ions considered in Sec. III. The approximation given by Eq. (31) works extremely well: the spectra cannot be distinguished on the scales used in the diagrams.

The expression of $\mathbf{d}(t)$ given by Walser *et al.* [21] is obtained by ignoring the nondipole corrections in the preexponential factor in the ionization amplitude (32) and the recombination amplitude (34) [31]. These additional approximations have no significant effect on the emission spectra for photons polarized along the laser polarization direction. Setting $1/c = 0$ in all three amplitudes in Eq. (31) leads to the formula obtained by Ivanov, Brabec, and Burnett [30] in the dipole approximation.

C. Classical electron trajectories

A simple physical interpretation can be given to the requirement that the detachment time t_d satisfy Eq. (19), as will now be discussed. We start with the classical analog of the Hamiltonian operator in Eq. (3),

$$H=\frac{1}{2}[\mathbf{p}+\mathbf{A}(\omega t)]^2+\frac{1}{c}(\hat{\mathbf{k}}\cdot\mathbf{r})[\mathbf{p}+\mathbf{A}(\omega t)]\cdot\mathbf{E}(\omega t), \tag{35}$$

obtained by replacing the operator $-i\nabla$ with the classical canonical momentum $\mathbf{p}$. The corresponding classical equations of motion are solved readily: If, at time t_0, the electron is located at the origin and has velocity $\mathbf{v}_0$, at time t_1 its position and velocity are, respectively,

$$\mathbf{r}(t_1)=\int_{t_0}^{t_1}dt''\mathbf{v}(t'') \tag{36}$$

and

$$\mathbf{v}(t_1)=v_\epsilon(t_1)\hat{\boldsymbol{\epsilon}}+v_k(t_1)\hat{\mathbf{k}}, \tag{37}$$

with

$$v_\epsilon(t_1)=\hat{\boldsymbol{\epsilon}}\cdot\mathbf{v}_0+[A(\omega t_1)-A(\omega t_0)]+\frac{1}{c}E(\omega t_1)\int_{t_0}^{t_1}dt''v_k(t'') \tag{38}$$

and

$$v_k(t_1)=\hat{\mathbf{k}}\cdot\mathbf{v}_0+\frac{1}{2c}[v_\epsilon(t_0)+A(\omega t_1)-A(\omega t_0)]^2-\frac{1}{2c}v_\epsilon^2(t_0). \tag{39}$$

The corresponding acceleration is $\dot{\mathbf{v}}(t_1)=\dot{v}_\epsilon(t_1)\hat{\boldsymbol{\epsilon}}+\dot{v}_k(t_1)\hat{\mathbf{k}}$, with

$$\dot{v}_\epsilon(t_1)=-E(\omega t_1)+\frac{1}{c}\dot{E}(\omega t_1)\hat{\mathbf{k}}\cdot\mathbf{r}(t_1)-\frac{1}{c}\dot{A}(\omega t_1)v_k(t_1) \tag{40}$$

and

$$\dot{v}_k(t_1)=\frac{1}{c}\dot{A}(\omega t_1)[v_\epsilon(t_0)+A(\omega t_1)-A(\omega t_0)]. \tag{41}$$

The first two terms on the right-hand side of Eq. (40) can be recognized as the acceleration imparted by the electric-field component of the laser, corrected to first order in $1/c$ for its spatial inhomogeneity in the propagation direction. The third term and the right-hand side of Eq. (41) describe the acceleration due to the Lorentz force, also to first order in $1/c$. A wave packet formed by a linear superposition of nondipole Volkov waves, Eq. (A4), which at time t_0 is localized at the origin and has velocity $\mathbf{v}_0$, follows the classical trajectory (36) [22].

Consider now an electron that is detached from the core at time t_0 with zero initial velocity in the polarization direction. In the recollision model, the electron follows a classical trajectory unperturbed by the atomic potential. A trajectory returning to the core leads to photon emission via recombination, with the energy of the emitted photon being the sum of the ionization potential and the kinetic energy of the electron at the time of recombination. Working within the dipole approximation, Lewenstein and co-workers [10] have shown

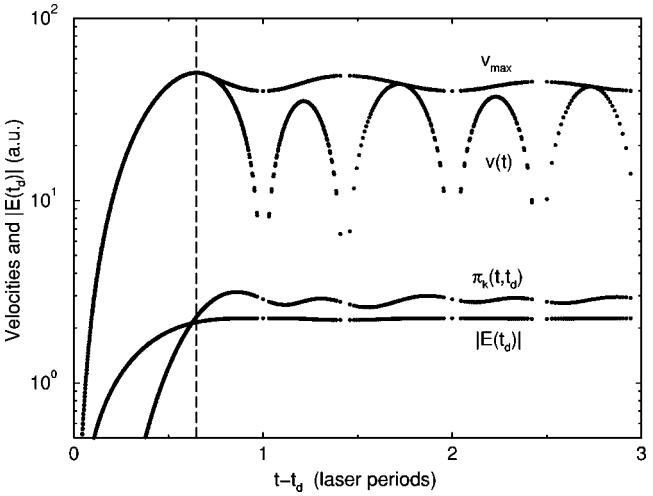

FIG. 1. Shown, for trajectories that return to the core, are (i) the electron's speed perpendicular to the laser polarization direction when it is detached, $|\pi_k(\mathbf{p}_s,t_d)|$; (ii) the electron's speed when it returns to the core, $v(t)$; (iii) its maximum speed between detachment and recombination, $v_{\max}$; and (iv) the strength of the electric field at the time of detachment, $|\mathbf{E}(t_d)|$. These quantities are plotted as functions of the duration of the trajectory, $t-t_d$, for a stationary field of 800 nm wavelength and intensity 1.8×10^{17} W cm^{-2}.

that there is a one-to-one correspondence between the classical trajectories of the recollision model and the saddle times obtained from Eq. (27). Such a correspondence also exists in our nondipole approach. In particular, it is straightforward to show that a necessary and sufficient condition for the electron to return to the origin at time t is that t_0 is any of the saddle times t_d defined by Eq. (19) and that $\mathbf{v}_0=\pi_k(\mathbf{p}_s,t_d)\hat{\mathbf{k}}$, where $\pi_k(\mathbf{p}_s,t_d)$ is defined by Eq. (21). In the classical model, $\pi_k(\mathbf{p}_s,t_d)$ is thus the velocity in the pulse propagation direction that the electron must have at the time of detachment, t_d, in order to return to the nucleus at the time of recombination, t. This initial velocity compensates exactly the displacement imparted by the magnetic-field component of the pulse on the free electron in the field [21].

How $|\pi_k(\mathbf{p}_s,t_d)|$ varies with $t-t_d$ is shown in Fig. 1, for a stationary field of 800 nm wavelength and 1.8×10^{17} W cm^{-2} intensity. Results are given for trajectories starting at equally spaced values of t_d. Few or no trajectories come back to the origin in certain time intervals, hence the gaps in the data. Also given in Fig. 1, for each trajectory, are the strength of the electric field at the time of detachment, $|\mathbf{E}(t_d)|$, the maximum speed the electron reaches between t_d and t, $v_{\max}$, and its speed at the time of recombination, $v(t)$. As will be seen below, all of these quantities are relevant for understanding the features of the nondipole spectra.

At this stage, we recall that the maximum kinetic energy of a returning electron in the dipole approximation is $3.17U_p$, where U_p is the ponderomotive energy. This maximum fixes the position of the cutoff frequency in the spectrum of emitted photons when nondipole effects are neglected [8–10]. The corresponding maximum velocity is indicated by the dashed vertical line in Fig. 1. Another well known fact is that several trajectories return with the same

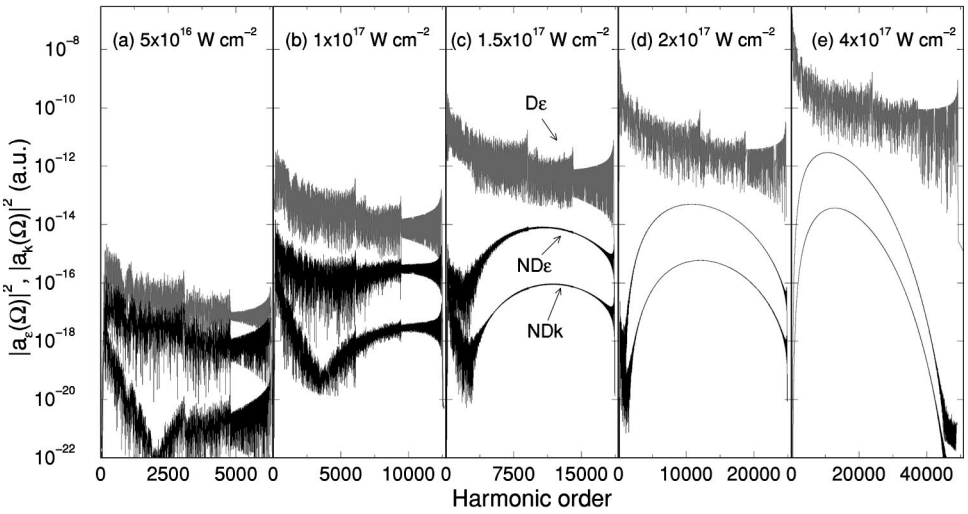

FIG. 2. The magnitude squared of the Fourier transform of the dipole acceleration (in a.u.) as a function of the photon energy (in units of $\hbar\omega$), for a Ne^{6+} ion interacting with a stationary laser field of wavelength 800 nm. Spectra for the emission of photons polarized along the laser polarization direction obtained in the dipole approximation (Dϵ) and in the nondipole nonrelativistic approximation (NDϵ) are shown, as well as the nondipole nonrelativistic spectra for photon emission polarized along the laser propagation direction (NDk).

kinetic energy during each half cycle, namely, a short trajectory (that lies to the left of the dashed line) and one or several long trajectories (that lie to the right of the dashed line). The long trajectories with return times of more than one period can give rise to intermediate plateaus and, through interference, to oscillations in the dipole spectrum.

We see in Fig. 1 that the behavior of the four plotted quantities is very different depending on whether the trajectory is long or short. In particular, for the short trajectories, the velocity $|\pi_k(\mathbf{p}_s,t_d)|$ and the magnitude of the electric field at the detachment time decrease rapidly with decreasing $t-t_d$. In addition, the electron attains its maximum velocity when it returns to the core. In contrast, for the long trajectories, $|\pi_k(\mathbf{p}_s,t_d)|$, $|\mathbf{E}(\omega t_d)|$, and the maximum velocity of the electron remain nearly constant close to their maximum allowed values. Note, in particular, that for the field considered in the figure, $|\pi_k(\mathbf{p}_s,t_d)|$, is about 3 a.u. for these trajectories.

III. RESULTS AND DISCUSSION

A. Nondipole effects in photon emission

Dipole and nondipole nonrelativistic spectra are compared in Figs. 2 and 3 for photon emission by multiply charged ions driven by a stationary 800-nm laser field. The modulus squared of the Fourier transform of the dipole acceleration is plotted against the effective harmonic order, Ω/ω. The Fourier transform of the dipole acceleration is defined as

$$\mathbf{a}(\Omega)=\frac{1}{(2\pi)^{1/2}}\int_T^{T+2\pi/\omega} dt\,\exp(-i\Omega t)\ddot{\mathbf{d}}(t), \qquad (42)$$

where T is chosen large enough so as to include the long trajectories that contribute to the dipole moment. We use the notation $a_\epsilon(\Omega)=\hat{\boldsymbol{\epsilon}}\cdot\mathbf{a}(\Omega)$ and $a_k(\Omega)=\hat{\mathbf{k}}\cdot\mathbf{a}(\Omega)$ for the components of the acceleration.

The gradual breakdown of the dipole approximation with increasing intensity is illustrated in Fig. 2 for emission by a Ne^{6+} ion ($I_p=207.3$ eV). Going from 0.5 to 4 $\times 10^{17}$ W cm^{-2}, the influence of the magnetic-field component first manifests itself as a reduction in photon emission polarized along $\hat{\boldsymbol{\epsilon}}$ as compared to the dipole approximation, then to a ''bending over'' of the plateaus, and finally to a marked suppression of emission at both ends of the spectrum and the disappearance of the intermediate cutoffs which separate the plateaus in the dipole approximation. A small shift in the position of the cutoffs is also noticeable.

Nondipole spectra for emission polarized parallel to the direction of propagation of the incident field are also shown in Fig. 2. Emission of photons polarized in this direction is forbidden in the dipole approximation. Compared to emission polarized along $\hat{\boldsymbol{\epsilon}}$, emission polarized along the propa-

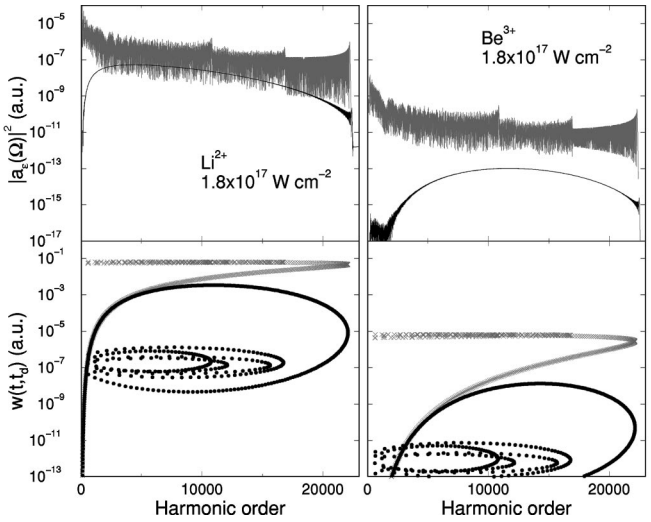

FIG. 3. The magnitude squared of the Fourier transform of the dipole acceleration (in a.u.) as a function of the harmonic order (upper plots). Results for the ions Li^{2+} and Be^{3+} in the dipole approximation (gray curves) and in the nondipole nonrelativistic approximation (black curves) are shown. The ions are irradiated by a stationary field of peak intensity 1.8×10^{17} W cm^{-2} and wavelength 800 nm. In the lower plots the ionization rate defined by Eq. (43), $w(t,t_d)$, is given for electron trajectories that return to the core, as a function of the harmonic order of the photon emitted at recombination. The dipole and nondipole values of $w(t,t_d)$ are indicated by crosses and circles, respectively.

gation direction is weaker, but the spectra are otherwise similar in most respects. The dip visible in the low-energy part of Figs. 2(a) and 2(b) also occurs when ions are driven by ultrashort pulses, and can be attributed to accidental cancellations between different terms contributing to the dipole moment [22].

In Fig. 2(a), we observe that $|a_\epsilon(\Omega)|^2$ is reduced by more than one order of magnitude compared to the predictions of the dipole approximation at the relatively weak intensity of 5×10^{16} W cm^{-2}. This reduction contrasts with the smaller decrease found for a Li^{2+} ion irradiated by a two-cycle 800-nm pulse of 9×10^{16} W cm^{-2} peak intensity [22,27], and the even smaller nondipole effects found for a He^+ ion irradiated by a 5-fs 800-nm pulse of 5×10^{16} W cm^{-2} peak intensity [21]. As will be seen later, the duration of the pulse influences to some degree the overall effect of the magnetic-field component on photon emission. However, the origin of the difference between the results of Fig. 2 and the results for He^+ and Li^{2+} can be attributed to the larger ionization potential of Ne^{6+}. That I_p plays an important role is demonstrated in the upper part of Fig. 3, where photon emission by Li^{2+} ($I_p=122.5$ eV) and Be^{3+} ($I_p=217.7$ eV) are compared for the same incident field [32]. Although the intensity is the same for both ions, the relative difference between the dipole and nondipole spectra is much less for Li^{2+}.

The strong dependence on I_p, and in fact all the major differences between the dipole and nondipole spectra, can be readily understood within the framework of the recollision model. Only two key quantities need to be considered: the effective detachment rate when the electron is born and its kinetic energy when it returns to the core. In the lower part of Fig. 3 we show, for each trajectory of Fig. 1, the detachment rate at time t_d of an electron with velocity $v_\perp \equiv \pi_k(\mathbf{p}_s,t_d)$ transverse to the electric field [33],

$$w(t,t_d)=\frac{4}{\pi}\frac{(2I_p)^3}{|E(\omega t_d)|^2}\exp\left[-\frac{2}{3}\frac{(2I_p+v_\perp^2)^{3/2}}{|E(\omega t_d)|}\right], \quad (43)$$

as a function of the harmonic order of the photon emitted at recombination, $[I_p+v^2(t)/2]/\omega$. We indicate the nondipole values of $w(t,t_d)$ by circles and the dipole values (obtained by setting $v_\perp=0$) by crosses. The rate (43) varies with the field in the same way as the square of the ionization amplitude (32), $a_{ion}^2(t,t_d)$, and has the same exponential dependence on I_p. Since the propagation and recombination amplitudes vary far less in magnitude than $a_{ion}(t,t_d)$ from trajectory to trajectory, the importance of the contribution to the spectrum of the different trajectories can be effectively gauged by the corresponding values of $w(t,t_d)$. As has been shown for He^+ interacting with a short laser pulse [34], much insight about the photon emission spectrum can be gained from this type of plot.

In the dipole approximation, $w(t,t_d)$ is largest for the long trajectories, as electrons having short trajectories are detached at lower electric fields. (See Fig. 1.) Therefore, short trajectories tend to contribute less to the photon emission spectrum. However, when the magnetic-field component of the laser field is taken into account, the opposite is true. This is due to the fact that $\pi_k(\mathbf{p}_s,t_d)$ is larger for the long trajectories than for the short ones. The exponential dependence of $a_{ion}(t,t_d)$ on the initial transverse velocity means that the ionization amplitude tends to be smaller for the long trajectories than for the short ones, and the latter end up dominating the spectrum over much of its range [20]. The secondary plateaus, which arise from the longest trajectories, almost completely vanish (although they still visibly contribute to the beryllium nondipole spectrum below $\Omega/\omega=2500$). The oscillations evident in the dipole spectrum largely disappear because at most frequencies only one set of trajectories (the short ones) significantly contribute to emission. The spectrum bends over as ionization is exponentially suppressed, due to the relatively small value of $|\mathbf{E}(t_d)|$ for the short trajectories that give rise to the lower harmonics, and to the large initial transverse velocity for the short trajectories that produce the high harmonics. Finally, the reduction in harmonic emission is proportionally larger for Be^{3+} than for Li^{2+} because the ionization amplitude varies faster with $v_\perp^2$ when I_p is larger.

We now evaluate the importance of the relativistic effects neglected in our approach by comparing, in Fig. 4, our nondipole nonrelativistic results with relativistic results recently obtained by Milošević, Hu, and Becker [20,24]. The case of a Ne^{6+} ion interacting with a stationary field of wavelength 1054 nm and intensities 0.7×10^{17} and 1.4×10^{17} W cm^{-2} is considered. Milošević's, Hu, and Becker's calculations are also done within the SFA but are based on the Klein-Gordon equation rather than on the Schrödinger equation. The relativistic results shown in the figure are the emission rates presented in Fig. 2 of Ref. [20], rescaled so as to facilitate comparison [35].

The large differences between the dipole and nondipole results indicate a strong influence of the magnetic-field component of the laser field for these parameters. As in Figs. 2(d) and 2(e), the nondipole spectrum is completely dominated by the short trajectories at 1.4×10^{17} W cm^{-2}. At this intensity, the maximum velocity of the electron, v_{max}, is at most 42% of the speed of light (i.e., $v_{max}^2/c^2=0.18$) for any returning trajectory. The good agreement between our nondipole nonrelativistic spectra and the relativistic spectra, aside from an arbitrary overall factor, suggests that the relativistic effects that are not taken into account in our model are not important. The difference is largest for the highest harmonics, as could be expected, since v_{max}^2/c^2 grows linearly with the energy of the photon emitted at recombination for electrons following short trajectories. Compared to the spectra obtained in the dipole approximation, the cutoffs occur at a slightly higher photon energy in the nondipole nonrelativistic calculation. The origin of this effect is the additional kinetic energy the returning electron acquires due to its drift along the pulse propagation direction. However, the nondipole nonrelativistic calculation neglects other effects, such as the increase in the inertial mass, which contribute to the kinetic energy to order $1/c^2$. In the relativistic results, these additional effects lead to a small displacement of the cutoffs to lower energies. We have verified that the classical calculations within the recollision model yield the same shifts as in

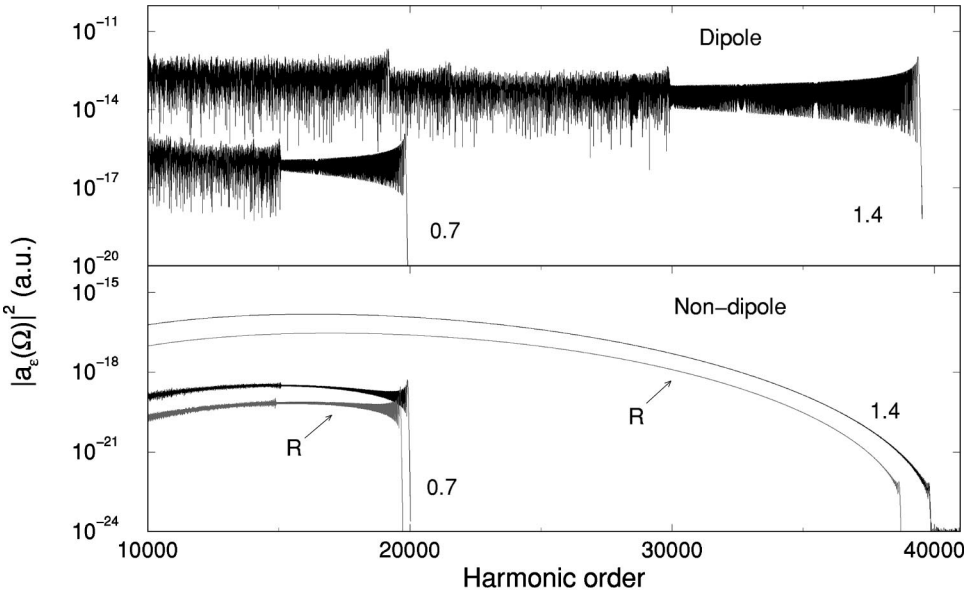

FIG. 4. The magnitude squared of the Fourier transform of the dipole acceleration (in a.u.) as a function of the photon energy (in units of $\hbar\omega$). Spectra for a Ne^{6+} ion obtained in the dipole and nondipole nonrelativistic approximations are shown for the emission of photons polarized along the laser polarization direction. The ion is irradiated by a stationary laser field of peak intensities 0.7 and 1.4×10^{17} W cm^{-2}, as indicated, and wavelength 1054 nm. The nondipole results are compared with the relativistic results (R) of Milošević, Hu, and Becker [20].

our nondipole nonrelativistic spectra and as in Milošević, Hu, and Becker spectra when the dynamics of the detached electron is described, respectively, by the Hamiltonian (35) and by the relativistic Lorentz equation. Finally, we note that $v_{\max}^2/c^2$ is less than 0.18 for the short trajectories responsible for the generation of photons below the harmonic order 30 000 at 800 nm wavelength, and is less than 0.10 for the short trajectories responsible for the strongest photon emission in Figs. 2 and 3. The relativistic effects neglected in our approach are therefore not expected to be significant at the intensities considered.

To conclude this section, we briefly discuss photon emission by ions driven by ultrashort pulses. Spectra for three- and four-cycle pulses are shown in the top and middle diagrams of Fig. 5. The field is described by Eqs. (1) and (2) with

$$f(\eta)=\sin^2\left(\frac{\eta}{2n}\right), \tag{44}$$

where n denotes the number of optical cycles of the pulse. The pulse is assumed to extend over all space. The corresponding Fourier transform of the dipole acceleration is

$$\mathbf{a}(\Omega)=\frac{1}{(2\pi)^{1/2}}\int_0^{2\pi n/\omega} dt\,\exp(-i\Omega t)\ddot{\mathbf{d}}(t). \tag{45}$$

The integral extends over the entire duration of the pulse instead of just one optical cycle as in the case of a stationary field. Results for a stationary field of the same intensity are shown in the bottom diagram. The plateau structure of the spectra for few-cycle pulses largely originates from the temporal variation of the intensity rather than from the contribution of very long trajectories [34]. (For every half-cycle during an ultrashort pulse, the trajectories are detached with different probabilities and return with different kinetic energies.) Overall, the magnetic-field component of an ultrashort pulse affects photon emission in a similar way as for stationary fields. However, for short pulses, photon emission is not as strongly suppressed at the low-energy end of the spectrum, and plateau structures with oscillations are still visible. This indicates that more than one electron trajectory is contributing to the emission of a particular harmonic in the largest part of the spectrum. Consider, for example, the low harmonics. As noted above, these are weak in the stationary case because they can be produced only through the return of an electron detached in a weak electric field. For few-cycle pulses, they can also be produced through the return of an electron detached near the end of the pulse, at a time where

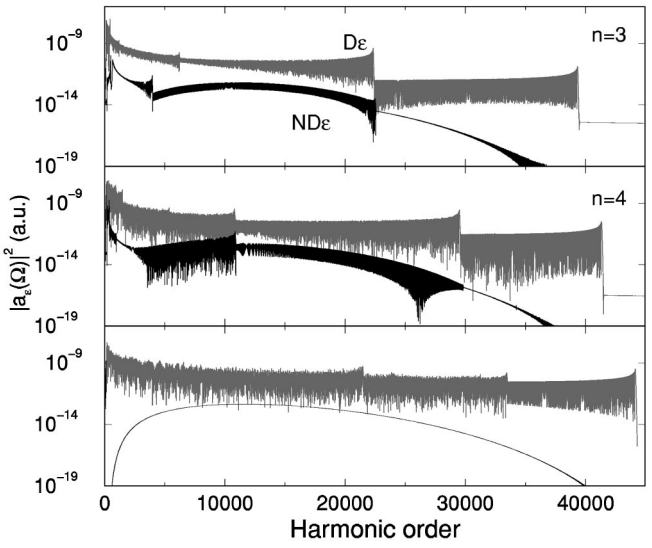

FIG. 5. The magnitude squared of the Fourier transform of the dipole acceleration (in a.u.) as a function of the photon energy (in units of $\hbar\omega$). Spectra for a Be^{3+} ion obtained in the dipole and nondipole approximations are shown for the emission of photons polarized along the laser polarization direction (Dϵ, NDϵ) for a three cycle pulse ($n=3$), a four cycle pulse ($n=4$), and a stationary field. The peak intensity is 3.6×10^{17} W cm^{-2} and $\lambda=800$ nm.

the electric field is strong but the intensity envelope of the pulse falls off rapidly. Since the falloff prevents it from attaining a high velocity, the electron can only contribute low-energy photons and is not deflected as much by the magnetic-field component of the pulse.

B. Selective compensation of the magnetic drift using a second laser pulse

At intensities where the dipole approximation is valid, the contribution of each electron trajectory to photon emission depends primarily on the electric-field strength at the time of ionization. At higher intensities, the contribution of a particular trajectory can be drastically reduced by the drift induced by the magnetic component of the field. As noted above, to return to the nucleus the electron must be emitted with a nonzero velocity transverse to the electric field, and the probability for this is exponentially small in the tunneling regime. At the intensities considered here, the Lorentz force acting on the electron has a magnitude comparable to that exerted by the electric-field component of a relatively weak laser field. This suggests that the magnetic drift can be compensated, at least for certain trajectories, by irradiating the ion with a second, weak laser field, polarized along the propagation direction of the intense one. In this section, we show by an example that a selective compensation of the magnetic drift through this mechanism is indeed possible.

We consider the case of a Ne^{6+} ion irradiated by a combination of two ultrashort pulses, both with the same carrier wavelength (800 nm). The first pulse, with vector potential $\mathbf{A}$, propagates in the direction $\hat{\mathbf{k}}$ and has the polarization vector $\hat{\boldsymbol{\epsilon}}$. The second pulse has the vector potential $\mathbf{A}_{\mathrm{w}}$ and the polarization vector $\hat{\boldsymbol{\epsilon}}_{\mathrm{w}}$, with $\hat{\boldsymbol{\epsilon}}_{\mathrm{w}} \equiv \hat{\mathbf{k}}$. We assume that the second pulse is weak enough to be treated in the dipole approximation. Therefore, the Schrödinger equation governing the motion of the electron in the nondipole nonrelativistic approach reads

$$i\frac{\partial}{\partial t}\Psi(\mathbf{r},t) = \left(\frac{1}{2}[-i\boldsymbol{\nabla} + \mathbf{A}(\omega t) + \mathbf{A}_{\mathrm{w}}(\omega t)]^2 + \frac{1}{c}(\hat{\mathbf{k}}\cdot\mathbf{r}) \times [-i\boldsymbol{\nabla} + \mathbf{A}(\omega t)]\cdot\mathbf{E}(\omega t) + V(r)\right)\Psi(\mathbf{r},t), \tag{46}$$

with $\mathbf{E}(\omega t) = -(d/dt)\mathbf{A}(\omega t)$. Within the SFA, the dipole moment of the ion can be still be expressed as in Eqs. (14) and (18), with the saddle momentum and the saddle times determined by Eqs. (15) and (17); however, we now have

$$\boldsymbol{\pi}(\mathbf{p},t) = \mathbf{p} + \mathbf{A}(\omega t) + \mathbf{A}_{\mathrm{w}}(\omega t) + \frac{1}{c}\left[\mathbf{p}\cdot\mathbf{A}(\omega t) + \frac{1}{2}A^2(\omega t)\right]\hat{\mathbf{k}}. \tag{47}$$

We assume that the two pulses have the same envelope, with the second pulse delayed by a time τ_{w} with respect to the first one. We take, specifically,

$$\mathbf{A}(\omega t) = \frac{\mathcal{E}}{\omega}\sin^2\left(\frac{\omega t}{2n}\right)\sin(\omega t)\,\hat{\boldsymbol{\epsilon}} \tag{48}$$

and

$$\mathbf{A}_{\mathrm{w}}(\omega t) = \frac{\mathcal{E}_{\mathrm{w}}}{\omega}\sin^2\left(\frac{\omega t - \delta}{2n}\right)\sin(\omega t - \delta)\hat{\mathbf{k}}, \tag{49}$$

where $\delta = \omega\tau_{\mathrm{w}}$ and n is the number of optical cycles encompassed by each pulse. In the classical model, an electron detached at a time t_{d} must have an initial velocity

$$\mathbf{v}_{\perp} = -\frac{1}{t - t_{\mathrm{d}}}\left\{\int_{t_{\mathrm{d}}}^{t} dt''[A_{\mathrm{w}}(\omega t'') - A_{\mathrm{w}}(\omega t_{\mathrm{d}})] + \frac{1}{2c}\int_{t_{\mathrm{d}}}^{t} dt''[A(\omega t'') - A(\omega t_{\mathrm{d}})]^2\right\}\hat{\mathbf{k}} \tag{50}$$

to return at the nucleus at time t. The electric-field amplitude of the second pulse, $\mathcal{E}_{\mathrm{w}}$, and the time delay τ_{w} are chosen so that $\mathbf{v}_{\perp} \approx 0$ for a particular group of trajectories.

The left panel in Fig. 6 shows the magnitude squared of the Fourier transform of the dipole acceleration of Ne^{6+} as a function of the photon energy for a two-cycle Ti:sapphire pulse with $\mathcal{E} = 3.2$ a.u. acting alone ($\mathcal{E}_{\mathrm{w}} = 0$). In order to illustrate more clearly the differences between the dipole and nondipole results, the fast oscillations in the spectra have been averaged by convoluting with a Gaussian window function. Let us first consider the trajectory of an electron ''born'' at time $t_{\mathrm{d}} = 116$ a.u. during the laser pulse. If the Lorentz force was negligible, the electron would return to the nucleus at time $t \approx 190$ a.u., where it could recombine with the emission of a photon of energy 7500ω. However, the Lorentz force is not negligible: in order to return the electron must have an initial velocity of about 2 a.u. opposite to the direction of propagation of the pulse. Correspondingly, $|a_{\epsilon}(\Omega)|^2$ is much reduced, compared to its value in the dipole approximation.

If, in addition, the ion is irradiated by a second two-cycle pulse, of field strength $\mathcal{E}_{\mathrm{w}} = 0.37$ a.u., and delayed by $\tau_{\mathrm{w}} = 62$ a.u. with respect to the first pulse, the electron returns to the core if detached with zero velocity at time $t_{\mathrm{d}} = 116$ a.u. In the center panel in Fig. 6 we see that the magnitude of the nondipole spectrum is now comparable to the spectrum obtained in the dipole approximation in the region of the 7500th harmonic. The small difference is due to the fact that the magnetic drift is compensated only for some of the trajectories that contribute to emission in this part of the spectrum, namely, those with $t_{\mathrm{d}} \approx 116$ a.u.

Photon emission in the region of the cutoff of the second plateau can be enhanced in a similar manner, by choosing the delay and the strength of the second pulse to be $\tau_{\mathrm{w}} = -80$ a.u. and $\mathcal{E} = 0.32$ a.u., respectively. The resulting spectrum is shown in the right panel of Fig. 6.

C. Single attosecond pulse generation

Finally, we investigate how the magnetic-field component of the laser pulse influences photon emission in the time

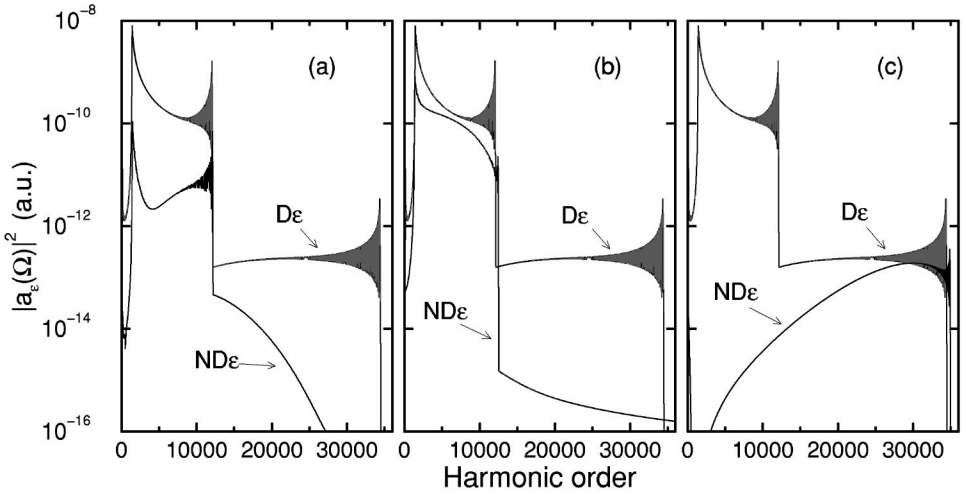

FIG. 6. The magnitude squared of the Fourier transform of the dipole acceleration, in a.u., of Ne^{6+} as a function of the photon energy (in units of $\hbar\omega$). The laser-pulse duration is two cycles, with peak intensity 3.6×10^{17} W cm^{-2} and wavelength 800 nm. Dipole (Dϵ) and nondipole (NDϵ) spectra are shown. In plots (b) and (c), the nondipole results are for the case in which the ion interacts with a second, weaker laser pulse polarized along the propagation direction of the intense pulse (see text). In plot (b), the time delay ($\tau_w=62$ a.u.) and intensity ($I_w=4.8\times10^{15}$ W cm^{-2}) of the second pulse were chosen such that photon emission in the neighborhood of the 7500th harmonic is enhanced, while in plot (c), $\tau_w=-80$ a.u. and $I_w=3.6\times10^{15}$ W cm^{-2}, leading to the enhancement of emission around the 30 000th harmonic.

domain. To this end, we calculate the frequency-resolved dipole acceleration for emission in a narrow frequency window centered about Ω, defined by [36]

$$a_\epsilon(t,\Omega)=\frac{1}{(2\pi)^{1/2}}e^{i\Omega t}\int_0^\infty d\Omega' e^{i(\Omega'-\Omega)t} \times F(\Omega'-\Omega)\hat{\boldsymbol{\epsilon}}\cdot\mathbf{a}(\Omega'), \quad (51)$$

where $F(\Omega'-\Omega)$ is a Gaussian window centered at $\Omega'=\Omega$. The square modulus of $a_\epsilon(t,\Omega)$ is shown in Fig. 7, for Ne^{6+} interacting with a four-cycle pulse of 3.6×10^{17} W cm^{-2} peak intensity at 800 nm wavelength. We concentrate on the emission of 3.9-keV photons ($\Omega=2500\omega$).

The results calculated in the dipole approximation are shown in Fig. 7(a). Each spike in this diagram corresponds to a burst of emission of 3.9-keV photons. The spikes occur precisely at the instants where, in the recollision model, detached electrons return to the nucleus with the speed required for emission at this energy. Seven bursts are particularly strong and have approximately the same intensity, showing that in the dipole approximation the emission is dominated by seven groups of trajectories.

However, the magnetic drift, when taken into account, changes this picture dramatically. The central part of the figure, where the nondipole results are plotted, shows that all but one of the seven returns that contribute most in the dipole approximation are severely suppressed. The only significant emission event occurs towards the end of the pulse and

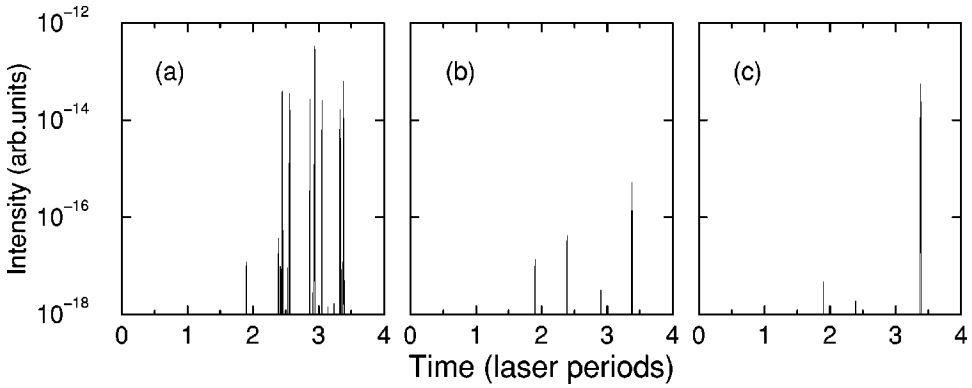

FIG. 7. The magnitude squared of the frequency-resolved dipole acceleration for photon emission centered about the 2500th harmonic of the driving field by a single Ne^{6+} ion interacting with a four-cycle Ti:sapphire pulse of 3.6×10^{17} W cm^{-2} peak intensity. Shown are results obtained in the dipole approximation (a) and in the nondipole nonrelativistic approximation (b),(c). Plot (c) shows the enhancement by a second laser pulse of photon emission at 3.4 laser periods. The peak intensity of the second pulse, I_w, is 2.2×10^{14} W cm^{-2} and the delay τ_w is 30.8 a.u.

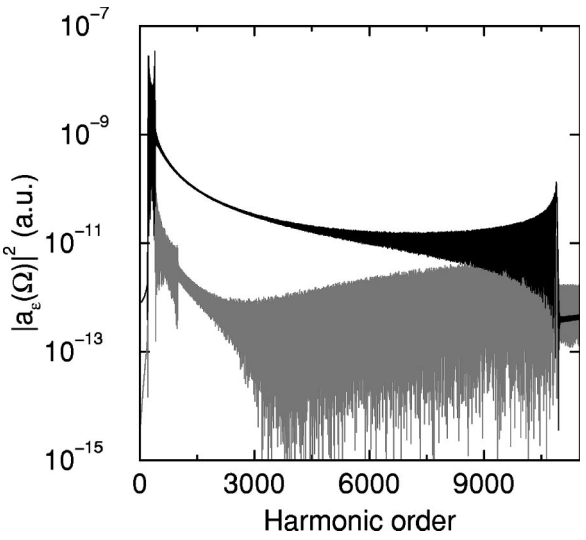

FIG. 8. The magnitude squared of the Fourier transform of the dipole acceleration of a single Ne^{6+} ion interacting with a four-cycle Ti:sapphire pulse of 3.6×10^{17} W cm^{-2} peak intensity. Shown are results obtained in the nondipole nonrelativistic approximation, with the upper curve illustrating the enhancement of photon emission around $\Omega/\omega=2500$ when the ion interacts with a second, weaker laser pulse having the same peak intensity and delay as in Fig. 7. The high-energy part of the spectrum is not shown.

dominates the spectrum. The corresponding trajectory is deflected less than the others, owing to the decrease in the strength of the magnetic-field during the trailing edge of the pulse. The width of the spike indicates that the duration of the burst is about 20 as. (It is worth noting that the intensity of this emission depends crucially on how the envelope of the pulse decreases at the end of the pulse: the slower the decrease, e.g., the longer the pulse, and the weaker the emission.) The other trajectories make a smaller contribution; their main effect is to induce, by interference, the oscillations in the nondipole spectrum which are visible in the lower curve of Fig. 8.

In Fig. 7(c), we present $|a_\epsilon(t,\Omega)|^2$ calculated for a superposition of the same intense pulse with another Ti-sapphire pulse, as discussed in Sec. III B. The electric-field amplitude of the second pulse, $\mathcal{E}_w$, and the delay between the two pulses, τ_w, are chosen so as to compensate the magnetic drift for the trajectory giving rise to the strongest burst of emission in Fig. 7(b). As seen from the diagram, when the magnetic drift is compensated, emission is as strong as in the dipole approximation. The other trajectories are further suppressed by the second pulse, with the consequence that a single attosecond pulse of x-ray photons is emitted. The same conclusions can be drawn from the corresponding spectrum, shown in Fig. 8. In fact, one sees from the spectrum that with the second pulse, emission is much more intense and occurs as a single burst (note the absence of oscillations), not only for $\Omega=2500\omega$ but also in a large range of frequencies around this value.

IV. CONCLUSIONS

In this paper we have given a detailed account of the approach introduced in Refs. [21,22] for describing photon emission by ions interacting with laser fields (stationary or pulsed) whose peak intensities are sufficiently high so that the dipole approximation is no longer applicable. This approach can be viewed as a nondipole generalization of the SFA theory of Lewenstein and co-workers [1,10]. It applies to the dynamical regime that lies between the usual nonrelativistic dipole regime and the fully relativistic regime. Using the nondipole nonrelativistic Volkov wave functions (A4) and within the SFA, we have shown that the time-dependent dipole moment of the ion in the laser field, $\mathbf{d}(t)$, can be reduced to the simple form given by Eq. (18). Then through a series of approximations, none of which compromise the accuracy of the calculations in any significant way, we recover the expression for the dipole moment derived by Walser *et al.* [21], whereby $\mathbf{d}(t)$ is obtained as a sum over amplitudes arising from particular electron trajectories.

The trajectories satisfy two simple classical criteria. First, if the electron is detached at some earlier time t_d, its displacement along the polarization direction must be zero at time t. Second, at time t_d its velocity along the laser-pulse propagation direction, $v_\perp$, must be equal and opposite to the average velocity that the free electron acquires in the propagation direction due to the Lorentz force between the times t_d and t. These are, of course, nothing more than the conditions that must be imposed if a classical electron detached at time t_d is to return to the core at time t. One recognizes immediately the language of the recollision model, modified so as to account for the magnetic-field induced drift of the detached electron. As in the intensity regime where the dipole approximation is applicable, it follows that the main features of photon emission spectra can be understood from two key quantities, namely, the tunnel ionization rate when the electron is detached and the kinetic energy of the electron when it returns to the core. In contrast to the dipole approximation, the tunnel ionization rates now depend strongly on $v_\perp$, and in particular on its magnitude relative to I_p and the magnitude of the electric field at the time of detachment. The overall effect of the dependence on $v_\perp$ results, at sufficiently high intensities, is a strong suppression of photon emission. Only trajectories with $t-t_d$ and $|v_\perp|$ small contribute meaningfully to the emission spectrum. As was emphasized recently in Ref. [5], it is remarkable that multiphoton processes in atoms interacting with intense laser fields, processes that would at first sight appear to be exceedingly complex, can in fact be largely understood in terms of classical trajectories of electrons that are detached and then subsequently return to their parent ion. These processes, in addition, provide a fascinating example of a system whose dynamics lies at the interface between quantum and classical mechanics.

Typically, a number of electron trajectories contribute in a comparable way to photon emission in some frequency interval or to ATI spectra in some energy range. We have discussed a scheme whereby a second laser pulse can be used to control an individual electron trajectory. By the appropriate choice of the laser parameters, the effect of the drift induced by the magnetic-field component of the pulse can be compensated for a selected trajectory, and enhanced for others, leading to the emission of a single attosecond pulse of high-frequency photons. The scheme has similarities to the pro-

posal by Corkum, Burnett, and Ivanov for producing an isolated attosecond pulse, in which single returning trajectories are selected by a temporal variation of the ellipticity of the incident field [37].

Many of the issues regarding the consequences of the breakdown of the dipole approximation discussed here apply equally well to strong-field recollision processes leading to single and multiple ionization. For instance, the reduced recollision probability in the nondipole nonrelativistic regime means, as has recently been observed experimentally in nonsequential multiple ionization [38], that these processes are strongly suppressed at very high intensity. This could well impose a practical barrier to the experimental study of strong-field recollision processes at intensities where relativistic effects become important. The selective compensation of the effect of the magnetic drift by a second laser pulse, as discussed above, may offer a way to alleviate this difficulty.

ACKNOWLEDGMENTS

The authors thank D. B. Milošević for discussions concerning the nondipole results shown in Fig. 3 and for communicating the relativistic results shown in Fig. 4. This work was supported by the UK EPSRC.

APPENDIX: NONDIPOLE NONRELATIVISTIC VOLKOV WAVE FUNCTION

The required nondipole nonrelativistic Volkov Green's function can be expressed as

$$G_{\mathrm{V}}^{(+)}(\mathbf{r},t;\mathbf{r}',t') = -i\,\theta(t-t')\int d\mathbf{p}\,\Psi_{\mathbf{p}}^{\mathrm{L}}(\mathbf{r},t)[\Psi_{\mathbf{p}}^{\mathrm{L}}(\mathbf{r}',t')]^{*}, \tag{A1}$$

where the function $\Psi_{\mathbf{p}}^{\mathrm{L}}(\mathbf{r},t)$ is a solution of the time-dependent Schrödinger equation (TDSE) (4) with $V(r)=0$. Calling $\Psi_{\mathbf{p}}(\mathbf{r},t)$ the solution of the TDSE (3) with $V(r)=0$, introducing the wave function $\Psi'_{\mathbf{p}}(\mathbf{r},t)$ as

$$\Psi_{\mathbf{p}}(\mathbf{r},t) = \exp\left(\frac{i}{c}\left[-i\boldsymbol{\nabla}\cdot\mathbf{A}(\omega t)+\frac{1}{2}A^{2}(\omega t)\right](\hat{\mathbf{k}}\cdot\mathbf{r})\right)\Psi'_{\mathbf{p}}(\mathbf{r},t), \tag{A2}$$

and recalling that $\boldsymbol{\nabla}\cdot\mathbf{A}(\omega t)$ commutes with $\hat{\mathbf{k}}\cdot\mathbf{r}$, it is seen that

$$i\frac{\partial}{\partial t}\Psi'_{\mathbf{p}}(\mathbf{r},t) = \frac{1}{2}\left(-i\boldsymbol{\nabla}+\mathbf{A}(\omega t)+\frac{1}{c}\left[-i\boldsymbol{\nabla}\cdot\mathbf{A}(\omega t)+\frac{1}{2}A^{2}(\omega t)\right]\hat{\mathbf{k}}\right)^{2}\Psi'_{\mathbf{p}}(\mathbf{r},t). \tag{A3}$$

The Hamiltonian operator in Eq. (A3) commutes with the momentum operator, so that the TDSE is easily solved. Transforming back to the length gauge, the nondipole Volkov wave function reads

$$\Psi_{\mathbf{p}}^{\mathrm{L}}(\mathbf{r},t) = \frac{1}{(2\pi)^{3/2}}\exp\left(i\boldsymbol{\pi}(\mathbf{p},t)\cdot\mathbf{r}-\frac{i}{2}\int^{t}dt''[\boldsymbol{\pi}(\mathbf{p},t'')]^{2}\right), \tag{A4}$$

where $\boldsymbol{\pi}(\mathbf{p},t)$ is defined in Eq. (8). The nondipole Volkov wave function (A4) is also readily obtained by expanding the relativistic Volkov wave function in powers of $1/c$ and neglecting terms of orders $1/c^{2}$ and higher. It reduces to the familiar nonrelativistic, dipole Volkov wave function when $1/c\rightarrow 0$.

[1] P. Salières, A. L'Huillier, P. Antoine, and M. Lewenstein, Adv. At., Mol., Opt. Phys. **41**, 83 (1999).
[2] T. Brabec and F. Krausz, Rev. Mod. Phys. **72**, 545 (2000).
[3] P.M. Paul, E.S. Toma, P. Breger, G. Mullot, F. Augé, P. Balcou, H.G. Muller, and P. Agostini, Science **292**, 1689 (2001).
[4] M. Hentschel, R. Kienberger, C. Spielmann, G.A. Reider, N. Milosevic, T. Brabec, P. Corkum, U. Heinzmann, M. Drescher, and F. Krausz, Nature (London) **414**, 509 (2001).
[5] P. Salières *et al.*, Science **292**, 902 (2001).
[6] R.A. Bartels, A. Paul, H. Green, H.C. Kapteyn, M.M. Murnane, S. Backus, I.P. Christov, Y. Liu, D. Attwood, and C. Jacobsen, Science **297**, 376 (2002).
[7] J.L. Krause, K.J. Schafer, and K.C. Kulander, Phys. Rev. Lett. **68**, 3535 (1992).
[8] K.C. Kulander, K.J. Schafer, and J.L. Krause, in *Super-Intense Laser-Atom Physics*, edited by B. Piraux, A. L'Huillier, and K. Rzazewski (Plenum Press, New York, 1993), p. 95.
[9] P.B. Corkum, Phys. Rev. Lett. **71**, 1994 (1993).
[10] M. Lewenstein, P. Balcou, M.Y. Ivanov, A. L'Huillier, and P. Corkum, Phys. Rev. A **49**, 2117 (1994).
[11] W. Becker, S. Long, and J.K. McIver, Phys. Rev. A **50**, 1540 (1994).
[12] M.Y. Kuchiev, JETP Lett. **45**, 404 (1987).
[13] N. Milošević, A. Scrinzi, and T. Brabec, Phys. Rev. Lett. **88**, 093905 (2002).
[14] J.R. Vazquez de Aldana and L. Roso, Opt. Express **5**, 144 (1999).
[15] A.V. Kim, M.Y. Ryabikin, and A.M. Sergeev, Usp. Fiz. Nauk **169**, 58 (1999).
[16] N.J. Kylstra, R.A. Worthington, A. Patel, P.L. Knight, J.R. Vázquez de Aldana, and L. Roso, Phys. Rev. Lett. **85**, 1835 (2000).
[17] M.Y. Ryabikin and A.M. Sergeev, Opt. Express **7**, 417 (2000).
[18] J.R. Vazquez de Aldana, N.J. Kylstra, L. Roso, P.L. Knight, A.S. Patel, and R.A. Worthington, Phys. Rev. A **64**, 013411 (2001).
[19] V.D. Taranukhin, Laser Phys. **10**, 330 (2000).
[20] D.B. Milošević, S.X. Hu, and W. Becker, Phys. Rev. A **63**, 011403(R) (2001).
[21] M.W. Walser, C.H. Keitel, A. Scrinzi, and T. Brabec, Phys. Rev. Lett. **85**, 5082 (2000).
[22] N.J. Kylstra, R.M. Potvliege, and C.J. Joachain, J. Phys. B **34**, L55 (2001).

[23] V.D. Taranukhin and N.Y. Shubin, Quantum Electron. **31**, 179 (2001).

[24] D.B. Milošević, S.X. Hu, and W. Becker, Laser Phys. **12**, 389 (2002).

[25] A.M. Perelomov, V.S. Popov, and M.V. Terent'ev, Sov. Phys. JETP **24**, 207 (1967).

[26] N.B. Delone and V.P. Krainov, J. Opt. Soc. Am. B **8**, 1207 (1991).

[27] N.J. Kylstra, R.M. Potvliege, and C.J. Joachain, Laser Phys. **12**, 409 (2002).

[28] D.B. Milošević, in *Super-Intense Laser-Atom Physics*, edited by B. Piraux and K. Rzążewski (Kluwer Academic, Dordrecht, 2001), p. 229.

[29] V.A. Borovikov, *Uniform Stationary Phase Method* (The Institution of Electrical Engineers, London, 1994).

[30] M.Y. Ivanov, T. Brabec, and N. Burnett, Phys. Rev. A **54**, 742 (1996).

[31] In the notation of Ref. [21], $P_x(t,t_0)$ and $P_z(t,t_0)$ are identical, respectively, to $\hat{\boldsymbol{\epsilon}}\cdot\mathbf{p}_s$ and $\hat{\mathbf{k}}\cdot\mathbf{p}_s$, where $\mathbf{p}_s$ is defined by Eq. (25) and $P_{zd}\equiv-\pi_k(\mathbf{p}_s,t_d)$. We take that the equation defining $S_m(t,t_0)$ in Ref. [21] should read $S_m(t,t_0)=(1/2m)\int_{t_0}^{t}dt'\{P_z(t,t_0)-e/(mc^2)[P_x(t,t_0)A(t')-e/(2c)A^2(t')]\}^2$.

[32] The nondipole nonrelativistic spectrum for Li^{2+} shown in Fig. 3 is in excellent agreement with the results of a recent, unpublished relativistic calculation [D.B. Milošević (private communication)].

[33] The exponential factor appearing in Eq. (43) was derived by Delone and Krainov [26]. It is multiplied by a preexponential factor which ensures that the integral of $w(t,t_d)$ over $v_\perp$ in the plane normal to $\mathbf{E}(\omega t_d)$ is identical to the total rate of ionization of an hydrogenic ion of binding energy I_p in a static electric field $\mathbf{E}(\omega t_d)$, as given by the familiar tunneling formula [L.D. Landau and E.M. Lifshitz, *Quantum Mechanics: Non-Relativistic Theory* (Pergamon, Oxford, 1977)].

[34] R.M. Potvliege, N.J. Kylstra, and C.J. Joachain, J. Phys. B **33**, L743 (2000).

[35] The rates of Ref. [20] are proportional to the square of the modulus of the Fourier transform of $\mathbf{d}(t)$ multiplied by the cube of the frequency of the emitted photon, Ω [D.B. Milošević (private communication)]. In order to compare them with the values of $|a_\epsilon(\Omega)|^2$ we have obtained, the rates have been multiplied by Ω and an arbitrary numerical factor. (The same factor is used for both intensities.)

[36] K.J. Schafer and K.C. Kulander, Phys. Rev. Lett. **78**, 638 (1997).

[37] P.B. Corkum, N.H. Burnett, and M.Y. Ivanov, Opt. Lett. **19**, 1870 (1994).

[38] M. Dammasch, M. Dörr, U. Eichmann, E. Lenz, and W. Sandner, Phys. Rev. A **64**, 061402(R) (2001).